The Astrophysical Journal Supplement Series, 174:136–144, 2008 January

GEMS SURVEY DATA AND CATALOG

John A. R. Caldwell,[1,2] Daniel H. McIntosh,[3] Hans-Walter Rix,[4] Marco Barden,[4] Steven V. W. Beckwith,[4,5] Eric F. Bell,[4] Andrea Borch,[4] Catherine Heymans,[4,6] Boris Häußler,[4] Knud Jahnke,[4,7] Shardha Jogee,[1,8] Klaus Meisenheimer,[4] Chien Y. Peng,[9,1] Sebastian F. Sánchez,[7,10] Rachel S. Somerville,[1,4] Lutz Wisotzki,[7] and Christian Wolf[11]

Received 2005 October 20; accepted 2007 June 14

ABSTRACT

We describe the data reduction and object cataloging for the GEMS survey, a large-area (800 arcmin^2) two-band (F606W and F850LP) imaging survey with the Advanced Camera for Surveys on the *Hubble Space Telescope*, centered on the *Chandra* Deep Field–South.

Subject headings: galaxies: evolution — galaxies: structure — surveys

1. INTRODUCTION

GEMS (Galaxy Evolution from Morphologies and SEDs) is a large-cycle-11 *Hubble Space Telescope* (*HST*) program aimed at mapping the evolution of the galaxy population through the combination of a large Advanced Camera for Surveys (ACS) imaging mosaic with ground-based information from COMBO-17 (Wolf et al. 2003). Rix et al. (2004) gave an overview, and many new results have already been obtained on red-sequence galaxies (Bell et al. 2004; McIntosh et al. 2005; Bell et al. 2006), active galaxies (Jahnke et al. 2004; Sánchez et al. 2004), bar and disk size evolution (Jogee et al. 2004; Barden et al. 2005), cosmological weak lensing (Heymans et al. 2005), and the cosmic evolution of ultraviolet luminosity density and star formation rate (Wolf et al. 2005; Bell et al. 2005). In this paper, we describe in more detail the GEMS data reduction and master catalog. The observations and data reduction steps, including the limiting magnitude achieved, are discussed in §§ 2 and 3. The detection and cataloging of objects, and the correlation of the GEMS source catalog with the COMBO-17 survey catalog are described in § 4. In § 5, we summarize how and where the GEMS data products can be accessed.

2. OBSERVATIONS

The GEMS collaboration was granted 125 orbits *HST* time during cycle 11 (GO-9500, PI: Rix) to image a large area centered on the Extended *Chandra* Deep Field–South [E-CDF-S; $\alpha, \delta\,(\mathrm{J2000.0}) = 03^{\mathrm{h}}32^{\mathrm{m}}25^{\mathrm{s}}, -27^{\circ}48'50''$] using the ACS Wide-field Camera (WFC). We constructed a tiling scheme (see Fig. 1) to obtain ~90% coverage of the $30' \times 30'$ E-CDF-S region, which had already been surveyed for rest-frame optical magnitudes and photometric redshifts by COMBO-17 (Classifying Objects by Medium-Band Observations in 17 Filters; Wolf et al. 2003).

The WFC (Ford et al. 2003) consists of a pair of 2048×4096 pixel ccd detectors separated by a 50 pixel gap. The pixels are 15 μm, and the plate scale is $0.05''$ pixel^{-1} for an overall extent of $\sim 202'' \times 202''$. The gain was set at 1 count per electron, and the a/d saturation level was 65536 counts. By virtue of the off-axis, few-element optical design, affording large area and high throughput, the detector pixel grid projects to a rhomboidally distorted grid pattern on the sky, in which the pixel size varies by a maximum of 19% in a fixed pattern. During data reduction, this geometric distortion is removed from the detector image to recover the true sky image.

The GEMS observations consisted of imaging in the F606W and F850LP passbands, hereafter referred to as V_{606} and z_{850}. Each *HST* visit consisted of three separate 12–13 minute exposures each for V_{606} and for z_{850}, dithered by ~3″ or ~60 pixel in a three-fold linear spacing that bridges the interchip gap of 50 pixel, and affords some subpixel sampling of the sky. In most visits the first orbit observed V_{606} and the second one z_{850}. The total exposure times were usually 2160 s for V_{606} and 2286 s for z_{850}, respectively, with the increase reflecting the rapid reacquisition possible in the second of two related orbits. A few observations obtained at a different spacecraft orientation (tiles 4, 6, 58) yielded integration times of 2286 s for V_{606} and 2160 s for z_{850} instead.

Contemporarily with the GEMS observing, the GOODS Project (Giavalisco et al. 2004) was observing their earliest of five data epochs, which also used the V_{606} and z_{850} passbands. Figure 1 illustrates the GOODS and COMBO-17 survey areas in relation to GEMS. The tiling pattern of the GEMS mosaic was designed to (1) encompass the 15 tile first epoch GOODS data, (2) create a large contiguous imaging field, and (3) avoid four extremely bright stars that would risk charge bleeding and widely scattered light on the detector. While GEMS-plus-GOODS corresponds to effectively 9×9 tiles, the central and bright star gaps result in a net of 63 GEMS tile locations, numbered as shown in Figure 1.

The calendar of GEMS data acquisition was as follows. First observed were tiles number 6 and 58 in 2002 September, with "orientat" (viz., the y-axis position angle on the resultant images) pointing nearly west (-92°). The bulk of the observations, all but four, were obtained in 2002 November with "orientat" nearly

[1] Space Telescope Science Institute, Baltimore, MD 21218; cyp@stsci.edu.
[2] McDonald Observatory, University of Texas, Fort Davis, TX 79734; caldwell@astro.as.utexas.edu.
[3] Department of Astronomy, University of Massachusetts, Amherst, MA 01003, dmac@hamerkop.astro.umass.edu.
[4] Max-Planck-Institut für Astronomie, D-69117 Heidelberg, Germany; rix@mpia.de, barden@mpia.de, bell@mpia.de, borch@mpia.de, boris@mpia.de, rachel@mpia.de.
[5] Department of Physics and Astronomy, Johns Hopkins University, Baltimore MD 21218; svwb@stsci.edu.
[6] University of British Columbia, Vancouver, BC, V6T 1Z1, Canada; heymans@physics.ubc.ca.
[7] Astrophysikalisches Institut Potsdam, D-14482 Potsdam, Germany; kjahnke@aip.de, meise@mpia.de, lwisotzki@aip.de.
[8] Department of Astronomy, University of Texas, Austin, TX 78712; sj@astro.as.utexas.edu.
[9] Department of Astronomy, University of Arizona, Tucson, AZ 85721.
[10] Centro Astronómico Hispano-Alemán Calar Alto, E-04004 Almería, Spain; sanchez@caha.es.
[11] Department of Physics, University of Oxford, Oxford OX1 3RH, UK; cwolf@astro.ox.ac.uk.

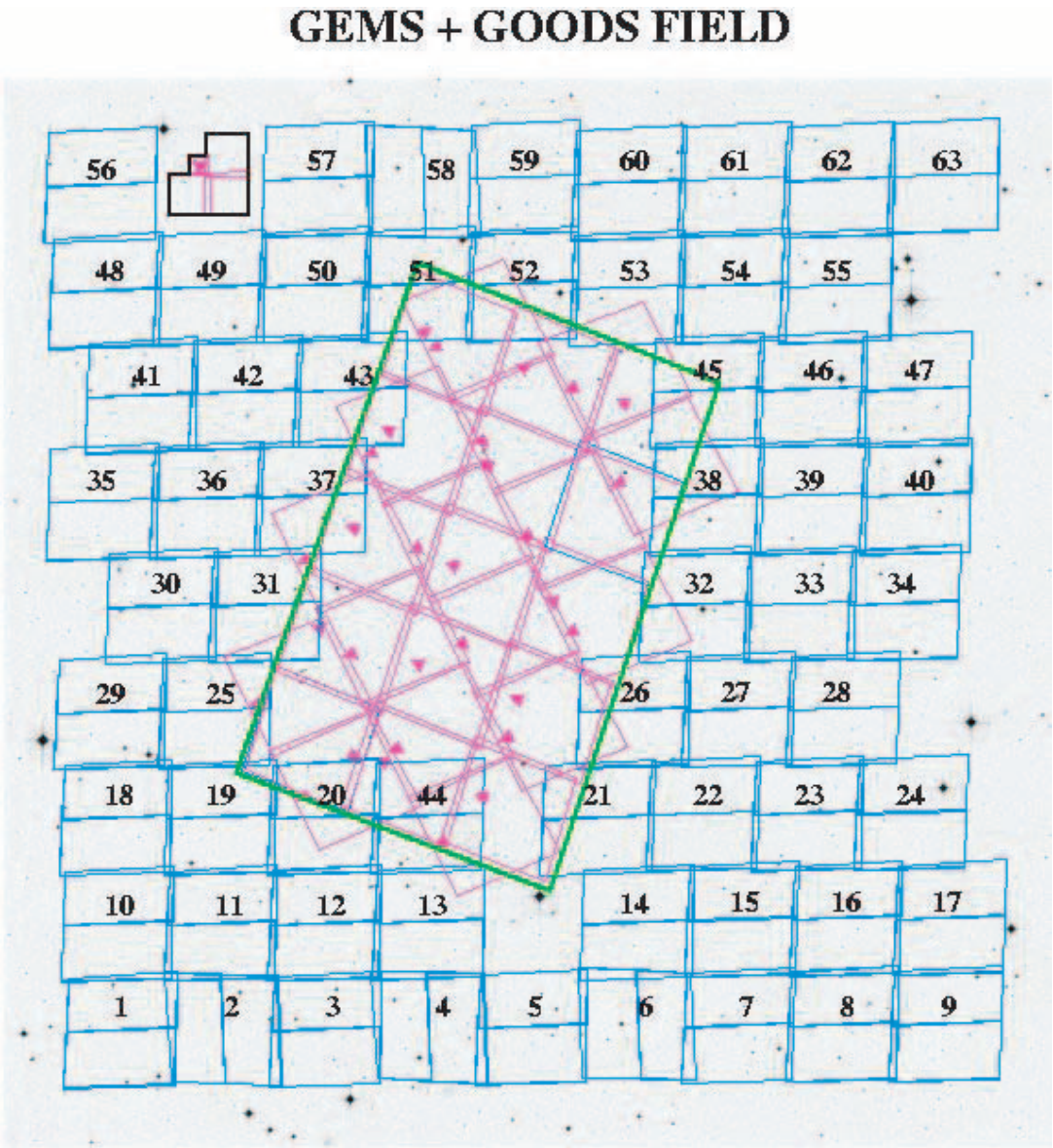

FIG. 1.—Layout of the GEMS image mosaic. With 800 arcmin^2, GEMS nearly covers the extended *Chandra* Deep Field–South from COMBO-17 (underlying *R*-band image), which measures $\sim 30' \times 30'$; the orientation is north up and east left. The individual GEMS tiles, labeled by their *HST* visit number, are shown as pairs of rectangles (ACS chips). The pink rectangular mosaic of 15 tiles at center delineates the GOODS first epoch that has been incorporated in the overall GEMS analysis (the lapped 16 pink tiles being later epochs and not used). The tilted large green rectangle indicates the area of SIRTF observations for GOODS. The much smaller size of the Hubble Deep Fields (located elsewhere on the sky) is indicated schematically at top left.

north (-2°). Last, tiles number 2 and 4 were observed in 2003 February with "orientat" nearly east (88°). The divergent orientations were dictated by guide star availability.

The tiles were chosen with an average overlap of $\sim 5''$ or ~ 100 pixel, which resulted in a total data area (including GOODS) amounting to $28.2' \times 28.2'$ (796 arcmin^2, or 84.3% of the $31.5' \times 30.0'$ COMBO-17 coverage; see § 4.2). The guiding stability is quantified by the rms guide star pointing corrections along the two orthogonal symmetry axes of the spacecraft, referred to as the V2 and V3 directions. These "guiding jitter" parameters were in the mean 3.6 and 4.7 mas, for V2rms and V3rms, respectively, with a standard deviation over all the exposures of 1.1 and 1.0 mas. This is excellent in relation to the pixel size of 50 mas. Note that one tile (chosen to be 44) could have only single-band data, due to the odd number of orbits. The execution of the observations encountered no difficulties and achieved uniformly excellent images.

3. DATA REDUCTION

The data were processed in two reduction versions: markI, to provide scientific-quality data as quickly as possible, and markII, to capitalize on any potential improvements enabled later on.

3.1. *MarkI Reduction*

The calibration of instrumental effects was done by the CALACS "on the fly" pipeline (Pavlovsky et al. 2003) as part of the data delivery from the MAST (Multimission Archive at Space Telescope) online service. The CALACS processing subtracted the overscan bias levels, the superbias image (produced from 7 days' intake of bias frames), and the time-scaled superdark image (produced from 1 day's intake of dark frames), and then divided by the flat field (calibrated by cluster aperture photometry done in orbit). The "super" frames achieve higher statistical accuracy by combining many measurements, yet secular

changes in the detectors, mostly from radiation damage, and practicality dictate a maximum useful time base. Finally, the gain was corrected to precisely unity, and the FITS header photometry keyword values inserted. In the markI reduction, the data were requested during 2002 August–2003 February, which invoked the version 4.1 of CALACS; the 2003 August–October markII reduction invoked version 4.3.

To remove the geometric distortion, all the exposures for a given tile and filter were drizzled (Fruchter & Hook 2002) onto a celestial pixel grid centered on the middle step of the z_{850} three-dither pattern for each pointing, using a version of the `multidrizzle` software (Koekemoer et al. 2003). In its basic function, the `multidrizzle` task flags bad detector pixels, subtracts the sky level, drizzles the flux from the detector grid onto the celestial grid, and then intercompares the result from the separate frames so as to flag cosmic rays and other transients and find the relative astrometric corrections to the nominal pointings. Unweighting all pixels flagged as invalid, and adding the small astrometric corrections to the nominal pointings, `multidrizzle` finally combines the input frames onto an output image of the weighted average (over only valid input pixels) of counts per second at each output pixel, which we call the science frame (or tile). A corresponding weight image is also produced, namely the effective exposure time contributing at each output pixel. The adopted weighting scheme disregards the weighting effect from the amplitude structure of the flat fields and from the interframe variations in sky level, which were judged to be a second-order refinement. Both the registration and the flagging of invalid pixels can be iterated, working backward from (i.e., redistorting, also referred to as blotting back) the existing best picture version. The output image scale was chosen to be $0.03''$ pixel^{-1}.

Cosmetic blemishes such as reflection ghosts, diffraction or scattering streaks, or cross-talk dips were left in the images. These defects had a sufficiently limited extent as to have negligible impact on the scientific usefulness of the images. The successful removal of cosmic rays by `multidrizzle`, without falsely flagging the centers of real objects, was checked visually. Its success was facilitated by the property that the data to be combined were always obtained within a single visit, resulting in very consistent exposure guiding. Thus, the estimated pointing coordinates as stored in the image headers were at least internally quite consistent between different dithers, although a modest external correction was needed (see § 3.3). A few faint asteroid trails are evident in the science output and weight images for the tiles V_{606} 29 and z_{850} 15 and 48. They stand out clearly in the weight image if `multidrizzle` recognized them as transient flux (in effect a long cosmic ray), but they stand out instead in the science image when they were so weak as to remain unrecognized by `multidrizzle`. Pixels that were saturated in the input frames were masked and thus contribute no weight to the final combined result.

The first epoch GOODS data on the *Chandra* Deep Field–South (CDF-S), consisting of a rectangle of 15 tile positions (see Fig. 1) at the center of the GEMS array, was reduced identically to the markI reduction of GEMS. The main differences were that the GOODS V_{606} data comprised two dither positions at each tile for a total exposure time of 1040 s, and the GOODS z_{850} data comprised four dither positions at each tile, for a total exposure time of 2120 s. Other than distinctions due to scaling from the somewhat different GOODS exposure times, the first epoch GOODS data were treated completely interchangeably with the GEMS data and will be included as an integral part of them for the rest of the paper.

3.2. *MarkII Reduction*

During the time interval between the markI and markII reductions, because of upgrades to site-installed software packages, the working version of `multidrizzle` had evolved. In addition, we made several changes in our working version of the software and in the configuration parameters that control the reduction, based on features in markI that we thought could be improved on, although the changes turned out to be mostly of a minor or cosmetic nature and do not imply any lesser scientific usefulness of the markI quantitative results. For example, satellite trails, being transients, had been flagged by `multidrizzle` in markI but their trail-edge wisps survived this cleaning procedure. In markII the program `satmask` (R. Hook 2004, private communication) was used to pre-excise the entire trail-affected locus before processing.

The effect of large bright objects on the sky subtraction and occasionally also on the calculated overscan level, was occasionally noted in markI by some small artificial steps in the calculated sky-subtracted zero level across the ccd amplifier quadrant boundaries. By experiment we adopted a better tuning of the sky level, 0.6(mode) + 0.4(median) over an entire chip (combining the quadrants having proved more robust). That still three of the tiles left with a serious zero level step that was rectified by rerequesting them under CALACS 4.4. This last CALACS version had been changed to remove the earlier vulnerability to extremely bright objects fortuitously near the ccd chip boundary, which were corrupting the nearby overscan region counts. The few markII frames needing that one feature from version 4.4 are otherwise homogeneous with the bulk requested under version 4.3, since the innovations in 4.4 do not change in any way the resulting calibrated WFC science array data.

One further innovation in the markII calibration was that CALACS now removed the differential scale effect due to the changing velocity aberration between exposures. Stacking exposures with the differential scale effect could cause an effective radial blurring (in markI relative to markII), but the 0.04 pixel maximum size of the effect for our data is negligible.

Finally, the drizzling kernel in markII was the lanczos (damped sync function) (Sparks et al. 2002), which suppresses one feature of the correlated noise that results from drizzling, namely the moiré pattern in the noise amplitude, that can be seen, for example, in the markI background level; markI used the square drizzling kernel (pixfrac = 0.8) that was available at the time. Therefore, the noise pattern in markII is smoother, but the noise remains correlated due effectively to an irreducible amount of angular averaging that is inherent in drizzling. Because of the sensitivity of lanczos algorithm to strong flux gradients, some purely cosmetic artifacts appeared only in markII at the centers of extremely saturated stars. The lanczos kernel furthermore does not behave well when operating on adjacent pixels with missing data. We are planning to reevaluate the choice of kernel and release the markII reduction publicly only with the best choice.

3.3. *Astrometric Registration*

The astrometry of each image tile was tied to the overall catalog from the ground-based COMBO-17 *R*-band image (Wolf et al. 2001) using the wcsfix program (R. Hook 2004, private communication). This relies on least-squares optimization of the position, orientation, scale, and axis skew of each tile based on the catalog of objects found by SExtractor (Bertin & Arnouts 1996); it is basically identical to the registration checking of the different dithers within the `multidrizzle` program described above. All matched objects were initially included, then conservatively

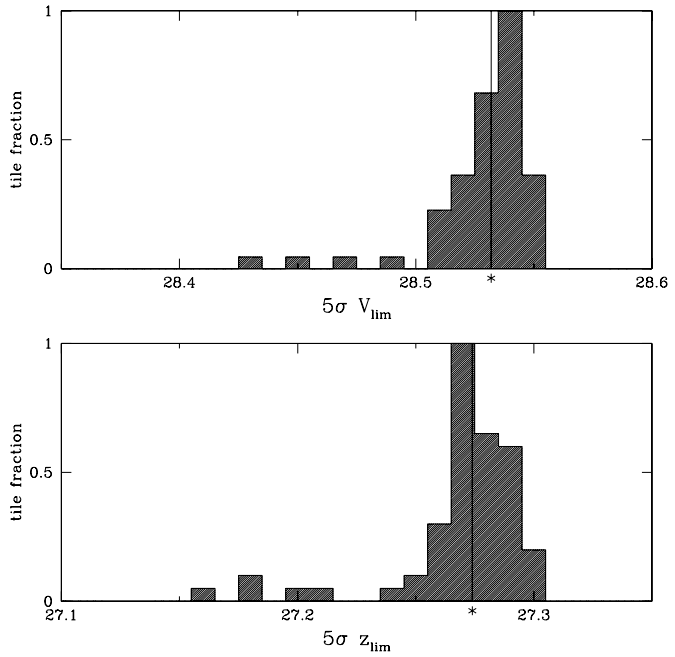

FIG. 2.—Histogram of the normalized number of GEMS tiles, vs. the 5 σ formal point source limiting magnitude estimated from the background noise level of the tiles. The asterisked vertical lines denote mean estimates of $V_{606} = 28.53$ and $z_{850} = 27.27$, respectively, which exclude the noisier tiles singled out in the text.

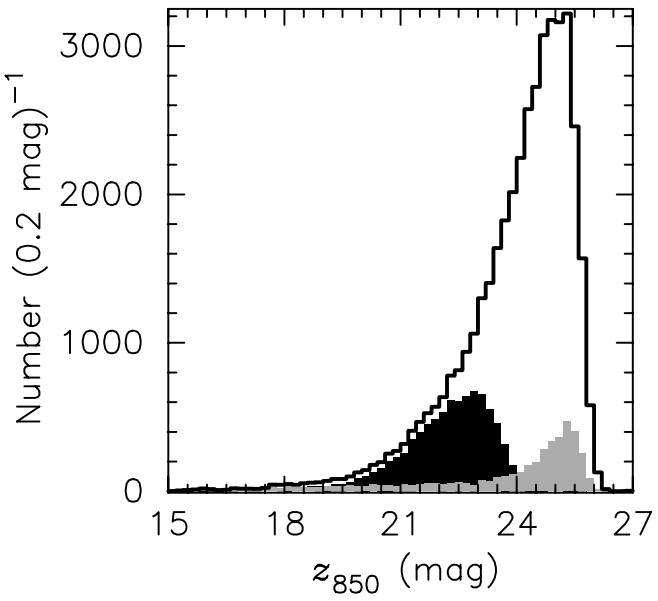

FIG. 3.—Source detections at z_{850} band in the GEMS *HST* image mosaic. For the full set of 78 ACS tiles we plot the 41,681 unique sources (*black outline*) from combining the "cold" and "hot" configuration SExtractor catalogs (see text for details). In addition, we show the subset of 8565 SExtracted sources matched to COMBO-17 galaxies with $R_{ap} \leq 24$ mag (*black filled distribution*), and the subset of 2251 likely stellar sources with SExtractor CLASS_STAR > 0.1 (*gray filled distribution*).

clipped for outliers. The V_{606} frames had a median of 164 objects bearing on the astrometric registration, with an x and y registration standard deviation of the mean of 0.21 and 0.20 pixel (at $0.03''$ pixel^{-1}). The z_{850} frames had a median of 89 useful objects with an x and y registration standard deviation of the mean of 0.24 and 0.25 pixel, respectively. The median absolute value size of the shifts needed to correct the instrument pointing reported in the observation header, was 55 pixel or $1.6''$ in x, 18 pixel or $0.54''$ in y, and 0.010° of rotation.

Both filters of each GEMS tile are thus tied to the COMBO-17 frame independently, with an relative uncertainty of typically 0.2 pixel. The absolute astrometric uncertainty is that of COMBO-17. For this Wolf et al. (2004) cite "better than" $0.15''$ as an global figure, but caution that errors approaching $0.3''$ are possible in some localized regions, which would raise the astrometric error of the coinciding GEMS tiles. To improve the source color distribution accuracy for proposed applications, a second version of the V-band frames was generated by *microregistering* with the IRAF `imshift` command and the SExtractored object position lists, to eliminate the very small remaining picture shift with respect to the z_{850}-band picture. This entailed an xy-shift with a uncertainty on the order of 0.02–0.03 pixel at the $0.03''$ pixel^{-1} scale. The effective precision of the V_{606} registration was 0.0245 pixel or 0.735 mas in the median, and the typical shift size was 0.38 x-pixel and 0.82 y-pixel in median absolute magnitude.

3.4. *Limiting Magnitude*

Because the noise correlation in the markII-reduced data were more spatially uniform, these were used to gauge the limiting magnitude of GEMS. The edge zone (not covered by all three dithers) was pared off and only the lower 90% of the data values were used (thus eliminating all objects including outer halos). Then the scatter per point was determined and adjusted upward appropriately for the lower 90% of a normal distribution. This results in a conservatively high estimate of the scatter, but one unaffected by objects. The 5 σ 3×3 input pixels (5×5 output pixels) limiting magnitude was then calculated for each tile. A correction of -0.80 mag was added to account for noise correlation based on Casertano et al. (2000, eq. [A13]). The results in Figure 2 are consistent with a uniform AB limiting magnitude (5 σ, point sources) of $V_{606} = 28.53$ and $z_{850} = 27.27$, except for a few tiles with slightly more scatter. Tile 56 is affected by a very prominent scattered light swath from its northwestern bright star. The other "hotter" tiles, 2, 4, and 40 may be showing the effect of a small bias subtraction jump between quadrants. The range in the limiting magnitude estimates is quite small.

Despite verifying homogeneity, these formal point source detection depths from background scatter are well over a magnitude fainter than the corresponding turnovers in the number counts (Figs. 3 and 4), which reflect the real detection limits from SExtractor. Thorough simulations of the recovery of artificial objects in simulated GEMS data have been carried out (Barden et al. 2005; McIntosh et al. 2005; B. Häußler et al., in preparation), including an analysis of the completeness for sources with realistic distributions of properties for this context. The present SExtractor detection setup was optimized for our science goals and is consistent with the resulting extended object completeness. Retuning SExtractor to detect the hypothetically faintest possible stars, i.e., to quantify the formal point source completeness, would correspond to seriously overdeblending (see § 4.1) the brighter extended sources and has thus been outside the scope of the project.

4. SOURCE CATALOG

The science goals of GEMS have relied on an empirical database of structural and morphological properties for a large and complete sample of distant galaxies for which redshifts and rest-frame quantities exist from COMBO-17. Therefore, the initial fundamental steps were cataloging of GEMS source detections from the *HST* imaging and matching these to their counterparts in the COMBO-17 catalog.

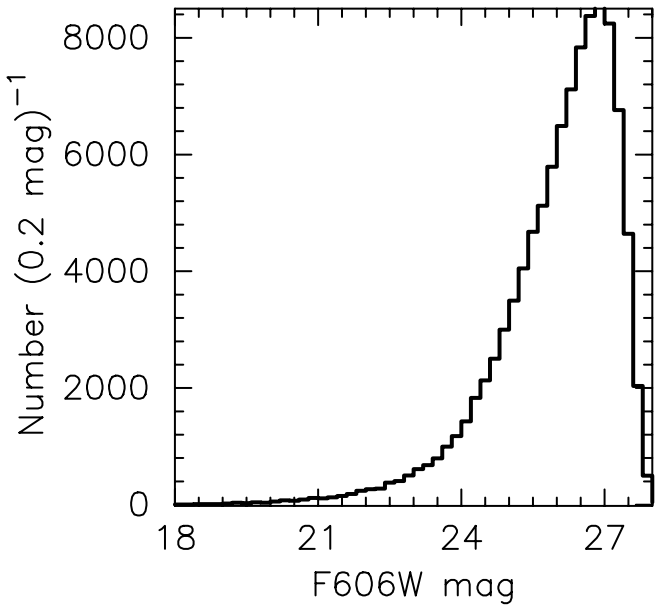

FIG. 4.—Source counts in the GEMS V_{606} mosaic from 77 ACS images. We detect 102,138 unique sources using the two-step "cold" and "hot" SExtractor method, with slightly modified configuration parameters (see Heymans et al. 2005). The increased number of detections compared to the z_{850} mosaic (see Fig. 3) is the result of the greater (by 1.2 mag) sensitivity of the V_{606} imaging.

4.1. *Object Detection*

Object detection and cataloging were carried out automatically on the GEMS astrometrically calibrated tiles with the SExtractor V2.2.2 software (Bertin & Arnouts 1996). SExtractor identifies sources and provides their image position, celestial coordinates, projected geometry, and flux parameters, down to a completeness cutoff that is as uniform as possible over the area. Moreover, SExtractor produces a segmentation map that parses the image pixels into those belonging to the extracted sources and the background sky, which is necessary for fitting galaxy surface brightness profiles with codes such as GALFIT (Peng et al. 2002) and GIM2D (Simard et al. 2002). We have chosen the 0.03″ scale z-band images to be the cataloging basis from consideration of the science goals. Before running SExtractor, the science images were converted from counts per second to counts, which are related to AB magnitudes via our adopted zero points ZP$[V_{606}]$ = 26.50482 and ZP$[z_{850}]$ = 24.84068. The conversion to counts is required for the correct SExtractor calculation of magnitude errors.

The use of SExtractor in effect defines the extracted sources; thus, the configuration file must be carefully tuned for the data set at hand to minimize both crediting noise as spurious objects, and rejecting believable objects. As it is common for objects to appear conjoined on the sky due to projection, further tuning of the configuration file is vital to avoid both the splitting (or "overdeblending") of essentially whole objects into pieces and the lumping together (blending) of different objects into spurious pseudo-objects. These considerations are controlled by four configuration parameters: (1) DETECT_THRESH, the detecting threshold above background; (2) DETECT_MINAREA, the minimum number of connected pixels above threshold; (3) DEBLEND_MINCONT, the minimum flux/peak contrast ratio to deblend separate sources; and (4) DEBLEND_NTHRESH, the number of deblending threshold steps.

The primary requirement of our SExtracting was to recover all $R_{\rm ap} \leq 24$ mag galaxies from COMBO-17 with the same spatial coverage. Fainter than this R-band aperture magnitude limit, COMBO-17 photometric redshifts become increasingly unreliable. Even with our well-defined source detection requirement, we have found that the large dynamic range of real objects occurring in the data makes it difficult to find any single configuration parameter set that gives a really satisfactory deblending outcome. This is especially so in the present case where the long-exposure ground-based images have reached low-surface brightness objects, and we are trying to find a match with space-based images that go especially deep for objects of relatively much smaller angular extent. To pick up the ~10% of $R_{\rm ap} \leq 24$ mag galaxies in COMBO-17 with the lowest surface brightness, the GEMS SExtractor detection threshold would need to be made so sensitive as to trigger many spurious object detections on substructural features within, and noise bumps in the outskirts of, bright objects (viz., "overdeblending"). Fortunately, as illustrated in Rix et al. (2004) we found that a two-pass strategy for object detection and deblending, using separate "cold" and "hot" SExtractor configurations, met our catalog requirements.

Given the size of the data set, it was essential that any deblending method be fully automatic. With this in mind, extensive tests to determine a combination of two detection configurations, which would maximize the number of $R_{\rm ap} \leq 24$ mag galaxies while minimizing the amount of overdeblending, were carried out independently by DHM and MB. Using five representative z_{850} tiles containing 837 $R_{\rm ap} \leq 24$ galaxies, a conservative cold configuration (DETECT_THRESH = 2.30, DETECT_MINAREA = 100, DEBLEND_MINCONT = 0.065, and DEBLEND_NTHRESH = 64) identified the high-surface brightness objects with negligible overdeblending, and a hot version (DETECT_THRESH = 1.65, DETECT_MINAREA = 45, DEBLEND_MINCONT = 0.060, and DEBLEND_NTHRESH = 32) then extracted the remaining faint low-surface brightness sources. All objects found in the hot run that overlapped the isophotal area of pre-existing cold run objects, were automatically discounted. For both configurations a weight map ($\propto$variance^{-1}) and a 3 pixel (FWHM) top-hat filtering kernel were used. The former suppresses spurious detections on low-weight pixels, and the latter discriminates against noise peaks, which statistically have smaller extent than real sources as convolved by the instrumental PSF. The final optimal configurations successfully detected 98.9% (828/837) of the COMBO-17 $R_{\rm ap} \leq 24$ galaxies with reliable deblending for 98.1%.

In addition to the detection parameters, the SExtractor configuration file includes two parameters used for a global estimate of the background sky level over a full image. A detailed explanation is provided in Bertin & Arnouts (1996). Briefly, SExtractor constructs a background map by splitting the image into a grid of background meshes of a given width (BACK_SIZE in pixels), applies a median filter of a given size (BACK_FILTERSIZE in pixels) to suppress possible local overestimates, iteratively clips the background histogram until its mean converges to within $\pm 3\,\sigma$ of its median value, and calculates the following mode:

$$\text{Mode} = 2.5 \times \text{Median} - 1.5 \times \text{Mean}. \quad (1)$$

Tests showed that using BACK_SIZE = 214 and BACK_FILTERSIZE = 5 on GEMS images provided a reasonable sky level estimation. The global background level and the rms pixel-to-pixel noise are given for each z_{850} frame in Table 1.

Our final catalog contains 41,681 *unique* GEMS z_{850}-band sources uniformly and automatically identified from 20,918 objects detected in the cold run, and augmented by 26,073 "good" objects found in the hot run (after rejection of the unwanted hot extensions to the pre-identified cold objects, described above).

TABLE 1

SOURCE DETECTION SUMMARY

Tile (1)	Background (2)	σ_{bkg} (3)	N_{cold} (4)	N_{hot} (5)	N_{good} (6)	N_{Rap24} (7)	θ_{sep} (8)	σ_{θ} (9)
GOODS 1	−0.164	4.46	173	419	407	84	0.10	0.10
GOODS 2	−0.155	4.48	186	454	446	103	0.13	0.09
GOODS 3	−0.135	4.50	199	430	417	117	0.13	0.12
GOODS 4	−0.139	4.47	226	516	499	117	0.13	0.11
GOODS 5	−0.161	4.50	274	582	558	127	0.14	0.11
GOODS 6	−0.168	4.49	194	451	440	115	0.12	0.11
GOODS 7	−0.119	4.48	233	507	501	140	0.12	0.11
GOODS 8	−0.101	4.46	183	431	419	95	0.16	0.12
GOODS 9	−0.208	4.45	246	552	538	134	0.15	0.11
GOODS 10	−0.166	4.44	242	593	582	151	0.15	0.12
GOODS 11	−0.113	4.48	198	474	460	112	0.14	0.11
GOODS 12	−0.176	4.46	231	534	520	127	0.13	0.12
GOODS 13	−0.156	4.47	263	562	557	138	0.15	0.10
GOODS 14	−0.206	4.45	271	566	559	145	0.12	0.10
GOODS 15	−0.112	4.43	249	537	522	136	0.11	0.12
GEMS 1	−0.114	3.88	235	590	577	102	0.14	0.12
GEMS 2	−0.169	4.28	246	545	535	129	0.14	0.12
GEMS 3	−0.102	3.88	312	679	663	141	0.13	0.12
GEMS 4	−0.138	4.25	250	595	584	139	0.13	0.12
GEMS 5	−0.075	3.90	306	666	639	140	0.12	0.10
GEMS 6	−0.143	4.08	290	601	584	151	0.12	0.10
GEMS 7	−0.077	3.90	285	628	611	115	0.12	0.12
GEMS 8	−0.172	3.92	239	581	557	94	0.14	0.14
GEMS 9	−0.120	3.89	271	614	601	122	0.13	0.11
GEMS 10	−0.100	3.87	239	543	535	106	0.12	0.11
GEMS 11	−0.113	3.83	217	576	570	112	0.17	0.13
GEMS 12	−0.085	3.84	255	674	608	106	0.12	0.08
GEMS 13	−0.094	3.88	236	586	575	130	0.14	0.13
GEMS 14	−0.079	3.92	293	649	630	126	0.11	0.11
GEMS 15	−0.103	3.90	282	613	599	123	0.11	0.10
GEMS 16	−0.087	3.88	297	647	641	124	0.13	0.12
GEMS 17	−0.152	3.87	334	793	768	157	0.10	0.10
GEMS 18	−0.132	3.86	252	639	628	110	0.13	0.10
GEMS 19	−0.091	3.90	248	592	568	104	0.16	0.12
GEMS 20	−0.108	3.86	215	526	514	95	0.12	0.12
GEMS 21	−0.112	3.87	303	700	684	151	0.12	0.10
GEMS 22	−0.100	3.87	307	647	634	140	0.12	0.11
GEMS 23	−0.113	3.82	238	651	635	95	0.20	0.11
GEMS 24	−0.097	3.90	265	648	630	103	0.12	0.11
GEMS 25	−0.110	3.89	299	669	661	131	0.14	0.11
GEMS 26	−0.102	3.89	271	638	622	118	0.11	0.11
GEMS 27	−0.088	3.83	251	638	631	102	0.13	0.12
GEMS 28	−0.116	3.84	268	622	612	113	0.12	0.12
GEMS 29	−0.213	3.92	263	638	612	104	0.12	0.10
GEMS 30	−0.142	3.88	323	736	697	138	0.14	0.10
GEMS 31	−0.129	3.87	282	620	600	126	0.14	0.10
GEMS 32	−0.145	3.88	258	612	606	104	0.15	0.13
GEMS 33	−0.092	3.88	299	703	684	149	0.14	0.11
GEMS 34	−0.047	3.87	277	589	580	111	0.12	0.11
GEMS 35	−0.108	3.91	335	731	714	155	0.11	0.09
GEMS 36	−0.095	3.89	298	666	648	144	0.13	0.10
GEMS 37	−0.143	3.86	237	616	605	116	0.13	0.12
GEMS 38	−0.120	3.84	316	707	692	128	0.11	0.08
GEMS 39	−0.112	3.89	292	734	713	152	0.13	0.11
GEMS 40	−0.108	3.93	292	614	599	140	0.17	0.12
GEMS 41	−0.178	3.99	349	711	697	162	0.11	0.11
GEMS 42	−0.145	3.94	298	644	626	128	0.13	0.10
GEMS 43	−0.150	3.94	316	683	666	145	0.13	0.13
GEMS 44	−0.050	3.89	238	547	533	125	0.11	0.10
GEMS 45	−0.040	3.95	315	712	701	152	0.13	0.12
GEMS 46	−0.153	3.94	295	706	691	126	0.15	0.11
GEMS 47	−0.168	3.92	284	673	656	120	0.13	0.11
GEMS 48	−0.132	3.90	268	653	637	106	0.13	0.10
GEMS 49	−0.087	3.90	243	554	549	101	0.14	0.11

TABLE 1—*Continued*

Tile (1)	Background (2)	σ_{bkg} (3)	N_{cold} (4)	N_{hot} (5)	N_{good} (6)	N_{Rap24} (7)	θ_{sep} (8)	σ_θ (9)
GEMS 50	−0.116	3.96	266	603	577	130	0.12	0.09
GEMS 51	−0.096	3.97	320	705	679	122	0.12	0.09
GEMS 52	−0.170	3.93	298	686	671	112	0.15	0.11
GEMS 53	−0.139	3.92	266	616	600	123	0.14	0.10
GEMS 54	−0.087	3.94	321	723	703	150	0.14	0.10
GEMS 55	−0.101	3.92	280	682	663	123	0.13	0.11
GEMS 56	−0.332	4.06	265	688	612	117	0.16	0.10
GEMS 57	−0.090	3.93	233	582	564	99	0.15	0.13
GEMS 58	−0.185	4.10	287	657	628	134	0.15	0.13
GEMS 59	−0.080	3.90	271	668	649	122	0.15	0.09
GEMS 60	−0.099	3.88	290	657	632	147	0.12	0.11
GEMS 61	−0.104	3.85	295	694	680	119	0.14	0.11
GEMS 62	−0.098	3.85	269	643	631	119	0.15	0.13
GEMS 63	−0.092	3.85	307	693	675	134	0.15	0.13
Totals			20918	48302	46991	9703		

NOTES.—For each z_{850} GEMS tile listed in col. (1), we give the global SExtractor estimate of the background sky level (col. [2]) and the rms pixel-to-pixel noise (col. [3]). The source extraction per tile is summarized by the raw number of "cold" (col. [4]), "hot" (col. [5]), and the combined cold and "good" hot (col. [6]) detections. The raw total of $N_{good} = 46{,}991$ includes 4522 duplicate and 394 triplicate source detections (see text for details). In addition, for each tile we give the number (col. [7]) of sources matched to $R_{ap} \leq 24$ mag galaxies from COMBO-17, and the mean (col. [8]) and rms (col. [9]) angular separation (in arcsec) between ACS and COMBO-17 coordinates.

The breakdown of cold, hot, and good sources per ACS frame is given in Table 1. The choice to analyze on a tile-by-tile basis, rather than mosaic-wise, resulted in 4916 sources (4522 duplicates, 394 triplicates) detected in multiple overlapping tiles as a result of their location near image boundaries. The most interior-located was selected for entry into the catalog resulting in the final total of 41,681 (i.e., $46,991 - 4522 - 394 - 394$).

The choice of z_{850} as the primary detection bandpass for cataloging followed from the importance of the morphology in the reddest bandpass for the science objectives. For some applications, e.g., weak lensing (Heymans et al. 2005), we have prepared a V_{606}-band catalog similarly as described above but with the hot configuration parameters adjusted as follows: (DETECT_THRESH = 1.4, DETECT_MINAREA = 37). The detectable source density is considerably higher in the V_{606} images, and the deblending more problematical due to the greater amplitude of substructure toward the blue. Figures 3 and 4 show the number counts of objects detected by GEMS in V_{606} and z_{850}, respectively.

4.2. *Cross-Correlation with COMBO-17*

The GEMS source catalog was cross-correlated in object coordinate space with the COMBO-17 source redshift catalog. For each GEMS source, a match was accepted for the nearest $R_{ap} \leq 24$ galaxy position within $0.75''$. For each tile, we tabulate in Table 1 the total number of $R_{ap} \leq 24$ mag galaxies, and the mean and rms angular separation θ_{sep} between the coordinate matches. From a total of 9703 matches there were 1138 cases of ambiguous matching; i.e., unique COMBO-17 sources with multiple GEMS detections from overlapping images as described in § 4.1. These were visually inspected and the best image detection selected; for 94% of these, the best case was the detection farthest from the image edge. Therefore, our final GEMS and COMBO-17 cross-correlated catalog contains 8565 unique $R_{ap} \leq 24$ mag galaxies, which yielded an rms positional agreement of $0.108''$ between the counterparts. Figure 5 shows the good astrometric correspondence between independently assigned COMBO-17 and GEMS object centroids, which is encouraging for the key goal of linking space and ground-based information. This comprises 85.2% of the 10,056 COMBO-17 sources in the E-CDF-S catalog with $R_{ap} \leq 24$ mag and classified as galaxies. The fraction agrees with the GEMS-to-COMBO area proportion (see § 2), a further indication that GEMS has reached the goal of detecting the COMBO-17 sample lying within the GEMS-plus-GOODS 796 arcmin^2 footprint.

Last, Figure 6 compares the relative number of GEMS detections per z_{850} magnitude bin that were matched to $R_{ap} \leq 24$ mag COMBO-17 galaxies with all detections that fall into the SExtractor automatic galaxy-like classification (i.e., CLASS_STAR ≤ 0.1). We stress that we do not use SExtractor for star/galaxy separation.

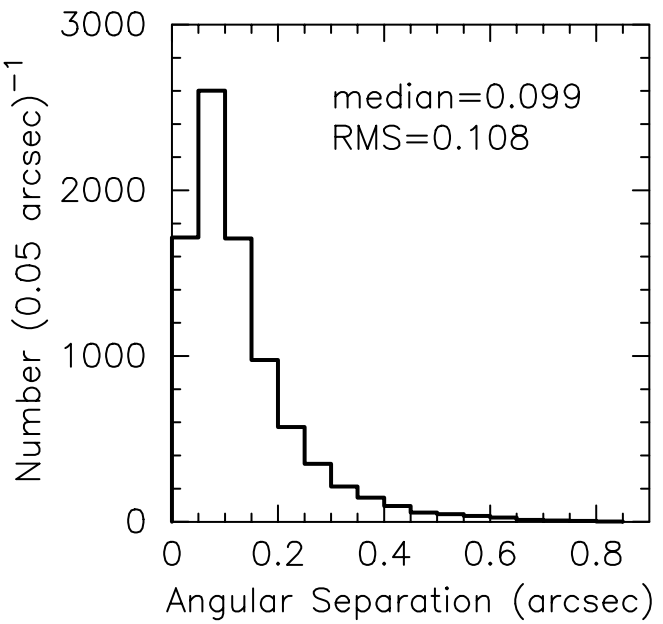

FIG. 5.—Distribution of angular separations between z_{850}-band ACS image and COMBO-17 source positions for the sample of 8565 cross-correlated galaxies. We provide the median and root mean square of the distribution.

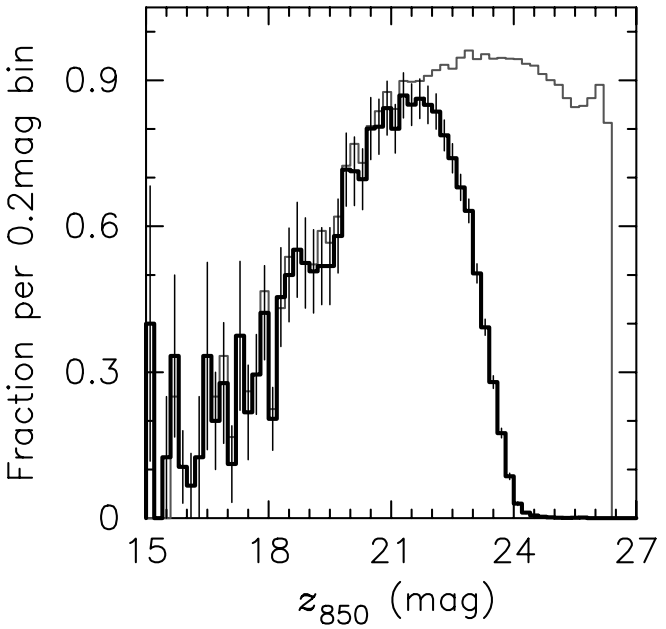

FIG. 6.—Fraction of all z_{850} SExtractor sources in GEMS that are known $R_{ap} \leq 24$ mag galaxies from COMBO-17 (*black with Poisson error bars*), and the fraction that are galaxy-like with SExtractor CLASS_STAR ≤ 0.1 (*gray*).

This comparison simply illustrates that statistically all bright extended sources from the GEMS images are matched to COMBO-17 redshifts. The z_{850} distribution for the 8565 COMBO-17 matches, and for CLASS_STAR > 0.1 sources, are given in Figure 3.

5. MASTER CATALOG AND DATA ACCESS

We produced a master catalog in FITS table format, which incorporates the GEMS and COMBO-17 information for the 8565 cross-identified objects. This master catalog was used for the GEMS science completed to date (see § 1). A small number of objects were found to be excludable from the GEMS science sample due to being, e.g., stars (72), too near the survey edge (33), or spoiled by the interchip gap (62). These sources are noted in the master catalog.

The GEMS master catalog and GEMS total source catalog will be published electronically in the STScI MAST archiving repository. We cite their contents here for reference. For all sources detected in the GEMS z_{850} imaging: (col. [1]) GEMS sexagesimal coordinate-based name; (cols. [2]–[3]) R.A. and decl. (J2000.0); (cols. [4]–[5]) total flux (SExtr. FLUX_BEST) and error; (cols. [6]–[7]) total magnitude (SExtr. MAG_BEST[12]) and error; (col. [8]) "local" background level; (col. [9]) isophotal area (SExtr. ISOAREA_IMAGE); (cols. [10]–[11]) image center x and y coordinates; (col. [12]) position angle (SExtr. THETA_IMAGE); (col. [13]) ellipticity; (col. [14]) image FWHM; (col. [15]) SExtractor FLAGS; (col. [16]) stellarity parameter (SExtr. CLASS_STAR); (col. [17]–[18]) ACS source and mask image names; (col. [19]) exposure time; (col. [20]) AB-mag zero point; (col. [21]) SExtractor Kron aperture radius; (cols. [22]–[24]) Cxx Cyy and Cxy SExtractor object ellipse parameters; (cols. [25]–[27]) blanks; (col. [28]) number of overlapping sources.

For the master catalog of sources cross correlated with COMBO-17, we provide COMBO-17 specific parameter names in parentheses.[13] The columns are as follows: (cols. [1]–[20]) as above; (col. [21]) COMBO-17 redshift (MC_z); (col. [22]) angular separation between ACS and COMBO-17 coordinates; (col. [23]) SExtr. MAG_BEST total R-band magnitude from COMBO-17 (Rmag); (col. [24]) number of overlapping sources; (cols. [25]–[26]) visual-band image x and y coordinates; (col. [27]) SExtractor Kron aperture radius; (cols. [28]–[30]) Cxx Cyy and Cxy SExtractor object ellipse parameters; (col. [31]) COMBO-17 object number (Seq); (col. [32]) COMBO-17 redshift uncertainty (e_MC_z); (col. [33]) COMBO-17 peak of redshift-estimate distribution (MC_z_ml); (col. [34]) COMBO-17 (0.3,0.7) luminosity distance (dl); (cols. [35]–[37]) COMBO-17 (0.3,0.7) Johnson M_U M_V and M_B VEGA-mags (UjMag VjMag and BjMag); (col. [38]) COMBO-17 (0.3,0.7) SDSS M_r (rsMag); (col. [39]) COMBO-17 R-band SExtr. MAG_BEST uncertainty (e_Rmag); (cols. [40]–[42]) COMBO-17 M_U M_V and M_B mag uncertainties (e_UjMag e_VjMag and e_BjMag); (col. [43]) COMBO-17 M_r mag uncertainty (e_rsMag); (col. [44]) COMBO-17 photometry flag (phot_flag); (col. [45]) COMBO-17 aperture Rmag (Ap_Rmag); (col. [46]) COMBO-17 R-band central surface brightness (mu_max); and (col. [47]) notes.

The MAST archive at the Space Telescope Science Institute makes the GEMS data products easily available via anonymous ftp.[14] The GEMS calibrated data so far stored at the MAST comprise the GEMS markI-reduced science and weight images for both V_{606} and z_{850} bands, and also the microregistered version (see § 3.3) of the V_{606} science and weight images. The markI-reduced first epoch GOODS science and weight images for both V_{606} and z_{850} bands, and the correspondingly microregistered V_{606} science and weight images are also stored there. A "readme" file provides details on the data files and a data summary table provides an overview of the details specific to each tile, too voluminous to cite here, such as the exposure date and time, celestial pointing coordinates and sky orientation, and the total sky level subtracted from combination of images at each tile location. The even more detailed accounting for the processing steps of each ccd chip is contained in the relevant FITS headers. The GEMS source catalog and the combined GEMS plus COMBO-17 master catalog, and any revised complete reduction (e.g., markII) will also be placed in MAST.

We thank Alison Vick and Guido de Marchi for support in preparing the *HST* observations. J. A. C. thanks Mauro Giavalisco (GOODS advice), Warren Hack and the entire STScI Computer Support staff (programming help), Richard Hook (satmask, wcsfix, wdrizzle), Anton Koekemoer (multidrizzle, wcsfix), and many other STScI colleagues, and finally the MAST (Multimission Archive at the Space Telescope) and CADC (Canadian Astronomy Data Centre) for their data services.

This research was supported by STScI through HST-GO-9500.01. Support for the GEMS project was provided by NASA through grant number GO-9500 from the Space Telescope Science Institute, which is operated by the Association of Universities

[12] We provide SExtractor MAG_BEST magnitudes for a rough estimate of the total F850LP-band flux of all GEMS galaxies. MAG_BEST is the optimum SExtractor magnitude depending on the degree of influence from neighboring sources. Nevertheless, SExtractor magnitudes are known to underestimate systematically the total flux of galaxies by about 10% (e.g., McIntosh et al. 2005), and we emphasize that they are not used in any GEMS science analysis.

[13] We refer the reader to the COMBO-17 Web site for additional details (http://www.mpia-hd.mpg.de/COMBOcombo_index.html).

[14] See the instructions at http://archive.stsci.edu/prepds/gems.

for Research in Astronomy, Inc. for NASA, under contract NAS5-26555. E. F. B. and S. F. S. acknowledge financial support provided through the European Community's Human Potential Program under contract HPRN-CT-2002-00316, SISCO (E. F. B.) and HPRN-CT-2002-00305, Euro3D RTN (S. F. S.). K. J. acknowledges support from the Deutsches Zentrum für Luft- und Raumfahrt (DLR) under project number 50 OR 0404. S. J. acknowledges support from the National Aeronautics and Space Administration (NASA) under LTSA grant NAG5-13063 issued through the Office of Space Science. D. H. M. acknowledges support from the National Aeronautics and Space Administration (NASA) under LTSA grant NAG5-13102 issued through the Office of Space Science. H. W. R. acknowledges support from the German-Israeli Science Foundation. C. W. was supported by the PPARC rolling grant in Observational Cosmology at University of Oxford.

REFERENCES

Barden, M., et al. 2005, ApJ, 635, 959
Bell, E. F., et al. 2004, ApJ, 600, L11
———. 2005, ApJ, 625, 23
———. 2006, ApJ, 640, 241
Bertin, E., & Arnouts, S. 1996, A&AS, 117, 393
Casertano, S., et al. 2000, AJ, 120, 2747
Ford, H. C., et al. 2003, Proc. SPIE, 4854, 81
Fruchter, A. S., & Hook, R. N. 2002, PASP, 114, 144
Giavalisco, M., et al. 2004, ApJ, 600, L93
Heymans, C., et al. 2005, MNRAS, 361, 160
Jahnke, K., et al. 2004, ApJ, 614, 568
Jogee, S., et al. 2004, ApJ, 615, L105
Koekemoer, A. M., Fruchter, A. S., Hook, R. N., & Hack, W. J. 2003, *HST* Calibration Workshop (Baltimore: STScI), 337
McIntosh, D. H., et al. 2005, ApJ, 632, 191
Pavlovsky, C. et al. 2003, ACS Instrument Handbook, ver. 4.0 (Baltimore: STScI)
Peng, C. Y., et al. 2002, AJ, 124, 266
Rix, H.-W., et al. 2004, ApJS, 152, 163
Sánchez, S. F., et al. 2004, ApJ, 614, 586
Simard, L., et al. 2002, ApJS, 142, 1
Sparks, W. B., Hack, W. J., Hook, R. N., & Koekemoer, A. M. 2002, STScI Instrum. Sci. Rep. ACS 2002-10 (Baltimore: STScI)
Wolf, C., Dye, S., Kleinheinrich, M., Meisenheimer, K., Rix, H.-W., & Wisotzki, L. 2001, A&A, 377, 442
Wolf, C., Meisenheimer, K., Rix, H.-W., Borch, A., Dye, S., & Kleinheinrich, M. 2003, A&A, 401, 73
Wolf, C., et al. 2004, A&A, 421, 913
———. 2005, ApJ, 630, 771